



UNIVERSITY OF LEEDS

This is a repository copy of *Simplified heat transfer model for highly active raffinate contained in buffer storage tanks*.

White Rose Research Online URL for this paper:

<https://eprints.whiterose.ac.uk/196242/>

Version: Accepted Version

Article:

Rahman, HS, Hunter, TN orcid.org/0000-0003-3922-491X and Heggs, PJ orcid.org/0000-0003-3209-6521 (2023) Simplified heat transfer model for highly active raffinate contained in buffer storage tanks. Chemical Engineering Research and Design (ChERD), 190. pp. 464-475. ISSN 0263-8762

<https://doi.org/10.1016/j.cherd.2022.12.013>

© 2022 Institution of Chemical Engineers. This manuscript version is made available under the CC-BY-NC-ND 4.0 license <https://creativecommons.org/licenses/by-nc-nd/4.0/>.

Reuse

This article is distributed under the terms of the Creative Commons Attribution-NonCommercial-NoDerivs (CC BY-NC-ND) licence. This licence only allows you to download this work and share it with others as long as you credit the authors, but you can't change the article in any way or use it commercially. More information and the full terms of the licence here: <https://creativecommons.org/licenses/>

Takedown

If you consider content in White Rose Research Online to be in breach of UK law, please notify us by emailing eprints@whiterose.ac.uk including the URL of the record and the reason for the withdrawal request.



eprints@whiterose.ac.uk
<https://eprints.whiterose.ac.uk/>

SIMPLIFIED HEAT TRANSFER MODEL FOR HIGHLY ACTIVE RAFFINATE CONTAINED IN BUFFER STORAGE TANKS

H. S. Rahman^{a,1*}, T. N. Hunter^a, P. J. Heggs^{a*}

^aSchool of Chemical and Process Engineering, University of Leeds, Leeds, U.K., LS2 9DT

¹Current affiliation - Sellafield Ltd, Hinton House, Birchwood Park Avenue, Warrington, Cheshire WA3 6GR

*Corresponding authors: haani.s.rahman@sellafieldsites.com, p.j.heggs@leeds.ac.uk

ABSTRACT

The research develops a simplified heat transfer model that allows prediction of the temperature response of the radioactive contents of the buffer storage tank at Sellafield. The model emanates from an energy balance around a singular tank with comprehensive analysis of the heat transfer phenomena. A converged solution has been demonstrated by comparing different numerical solution techniques. The model has been validated using measurements made at Sellafield indicating strong agreement in trends. The results indicate, whilst storing a full tank of radioactive liquor the vessel contents will not reach its boiling point of 95°C but will instead reach an equilibrium temperature of 89°C. The results also indicate that the model provides more accurate predictions compared with initial research at Sellafield. Simulations from the model revealed the tanks can safely store material for approximately 67% longer than is predicted by current practice. The model has been developed in Microsoft Excel ® and can be run with minimal computational power on any machine. It includes a user-friendly interface allowing operators to generate results from a range of scenarios by running simulations within minutes. The results generated from this model provide operations personnel with more information to influence decisions surrounding industrial-scale problems.

Keywords: Heat transfer; High-level waste management; Nuclear; Simplified heat transfer model; Highly active raffinate; Buffer storage

NOMENCLATURE

A	Area (m ²)	δ	Wall Thickness (m)
C_p	Specific Heat Capacity (J/kgK)	ρ	Density (kg/m ³)
d	Diameter (m)	μ	Dynamic Viscosity (kg/ms)
E	Thermal Effectiveness	σ	Stefan-Boltzmann Constant (W/m ² K ⁴)
g	Acceleration due to Gravity (m ² /s)	ν	Kinematic Viscosity (m ² /s)
h	Individual Heat Transfer Coefficient (W/m ² K)	ε	Emissivity
H	Characteristic Height (m)	Subscript	
k	Thermal Conductivity (W/mK)	c	Cooling Water
L	Characteristic Length (m)	I	Inside
\dot{M}	Mass Flow Rate (kg/s)	i	Coil Number
\dot{Q}	Heat Flow (W)	O	Outside
\dot{q}	Specific Heat Flux (W/m ²)	o	Initial
t	Time (s)	ves	Vessel
T	Temperature (K)	cell	Cell
T'	Temperature (°C)	HAR	Highly Active Raffinate
U	Overall Heat Transfer Coefficient (W/m ² K)	steel	Steel
V	Volume (m ³)	ull	Ullage region
Greek Letters		v	Vent
α	Thermal Diffusivity (m ² /s)	w	Wall
β	Thermal Expansivity (1/K)	r	Radiation
liq	Liquid	l	Loss
n	Iteration Number		
s	Surface	Dimensionless Numbers	
∞	Surroundings	Nu	$Nu = \frac{h_{i,e} d_{o,e,i}}{k_{c,i}}$, Nusselt Number
		Pr	$Pr = \frac{\nu}{\alpha}$, Prandtl Number
		Re	$Re = \frac{\rho u d}{\mu}$, Reynolds Number
		Gr	$Gr = \frac{g \beta (T_s - T_\infty) L^3}{\nu^2}$, Grashof Number

1. INTRODUCTION

This paper presents a simplified method for the prediction of the temperature response of holding tanks within a nuclear high level waste (HLW) buffer storage facility, specifically at Sellafield in the UK (formerly Europe's largest fuel reprocessing facility). Here buffer tanks accept highly active raffinate (HAR) liquid from reprocessing operations for storage, prior to being sent for further processing by evaporation and, eventually, vitrification. The buffer storage facility is part of the HLW management treatment process at Sellafield. HLW management refers to the treatment of a toxic, radioactive side-stream generated during the reprocessing of spent fuel from nuclear reactors. The HLW management process at Sellafield is presented in Fig. 1.

Spent nuclear fuel is reprocessed in the thermal oxide reprocessing plant (THORP). This generates recycled plutonium (Pu) and uranium (U) oxides, which can re-enter the fuel cycle, and an effluent stream of HAR). This is concentrated in evaporator vessels in the high active liquor evaporation and storage plant (HALES) (Shiels *et al.* 2018; Bux *et al.* 2017). This plant converts the stream into concentrated high activity liquor (HAL), which can then be processed in the waste vitrification plant (WVP) to produce a stable glass product more suitable for long-term storage.

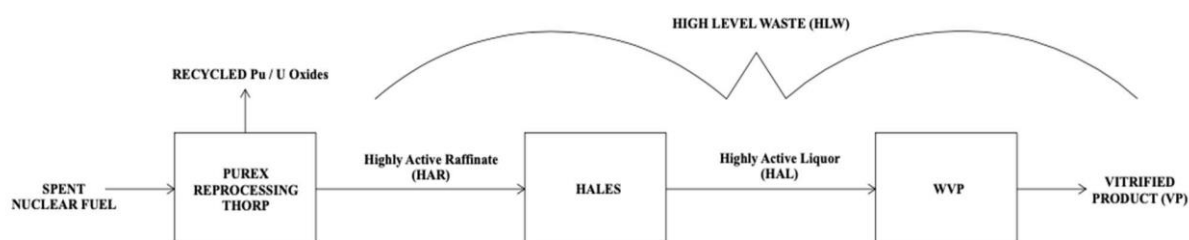


Figure 1. Schematic depicting the HLW management process for reprocessing liquors.

In order to maintain compliance with the Paris agreement, the world needs to eradicate its dependence on fossil fuels as an energy source (United Nations 2015). From the remaining energy options, nuclear remains one of the most accessible and low carbon power sources to date. As stipulated by many researchers in the sector, growth of the nuclear power industry relies on improvement in the understanding of nuclear legacy waste treatment mechanisms that allow safe disposal of radioactive material (Turvey and Hone 2000, Hanson 2014 and 2015). This research aims to enhance current understanding of the behaviour of legacy waste and provide information that contributes to the design of future HLW management facilities. The presented work addresses nuclear regulator recommendations for improved data on safety critical equipment on the site, and the information provided can inform and aid decisions regarding safety operations on the plant.

Both the evaporation and vitrification procedures have been well-researched throughout the literature to date (Panesar 2016; Alane and Heggs 2011; Barth *et al.* 2020). In particular, Panesar (2016) published an extensive analysis on the heat transfer mechanisms occurring within the Sellafield evaporators using computational fluid dynamics (CFD) software. Alane and Heggs (2011) examined the two-phase instabilities that exist during start-up of thermosyphon evaporators commonly employed in the nuclear industry. Barth *et al.* (2020) have developed a numerical model that can be applied to HLW vitrification processes. There have also been attempts to model the heat transfer mechanisms associated with long-term storage of solid HLW in a geological disposal facility. Zhou *et al.* (2020) present a layered three-dimensional heat conduction model that predicts the temperature at any point in the rock surrounding a single nuclear waste canister, while Case *et al.* (2020) proposed an analytical temperature solution satisfying the exponentially decaying boundary condition.

As indicated by the quoted literature, the science behind these operations on the Sellafield site is established and well understood. However, whilst the evaporation and vitrification plants have been thoroughly studied, there has been less interest throughout the literature in the temporary storage of nuclear effluent prior to evaporation. There have been some initial investigations on the temporary storage of nuclear effluent, where for example, Turvey and Hone (2000) discussed the heat transfer phenomena occurring in the Highly Active Storage Tanks (HASTs) as part of a safety assessment for the Radiological Protection Institute of Ireland. These tanks receive High Activity Liquor (HAL) that has been concentrated in the evaporators. In the analysis, Turvey and Hone reveal the structure of the heat loading for the HAST vessels as built in 1996. Each of the tanks have been designed such that, when active, heat loss through the cooling coils is the dominant mechanism in the HASTs. When the cooling coils are inactive, evaporative mechanisms begins to become the major contributor to heat loss and their impact is exacerbated as the temperature of the contents rises. At lower temperatures convective and thermal radiation heat losses can be considered significant in combination with the evaporative heat losses. Alternatively, this paper investigates heat transfer in buffer holding tanks for the effluent side-stream that is generated during the reprocessing of spent fuel prior to concentration, where the contained aqueous liquid is referred to as Highly Active Raffinate (HAR). Concentrated effluent which is received by the HASTs post evaporation is referred to as High Activity Liquor (HAL).

Temporary storage of HAR on the Sellafield site occurs in the buffer storage facility. The buffer facility was built for the purposes of in-tank evaporation of fission product raffinate from the original reprocessing plant at Sellafield. However, during times of high demand, the BSTs also act as buffer facilities for temporary storage of HAR until further evaporative capacity becomes available.

In addition to the stated literature concerning the simulation of heat transfer mechanisms occurring in nuclear processes, there is also a variety of publications that focus on the heat transfer occurring in

other more traditional industrial chemical processes and storage tanks. Dakkoune *et al.* (2020) investigated the temperature response behaviour of batch reactor systems, validating their simplified model against experimental measurements taken from a vessel hosting the perhydrolysis of formic acid. Johnson *et al.* (2021) presented a non-adiabatic model for jacketed agitated batch reactors experiencing thermal losses that does not require complex CFD software, while Ali *et al.* (2020) have published a simple 1-dimensional approach to the modelling of an industrial spray drying tower. Here, their work predicts the temperature of droplets within the tower as a function of the vertical position by formation of an energy balance equation. Collectively, this cited literature (Dakkoun *et al.* 2020; Johnson *et al.* 2021; Ali *et al.* 2020) presents modelling techniques for industrial chemical processes using a simplified approach that does not rely on complex CFD. There are many advantages to similar simplified approaches to modelling: The models developed produce fast simulations that can be used to collect data for a variety of applications and scenarios, and it leads to the production of user-friendly models that can be used without acquiring technical expertise in CFD. It also does not require expensive software and can be run on standard data handling software packages (e.g., MS ExcelTM) while they do not require large amounts of computational power.

There is a demand for improved data from, and simulation of, existing equipment that impinge on the safety of HLW treatment plants. These data and simulations can aid the design of future HLW plants, as well as allow for the safe operation of current facilities. In contrast to established simulations of evaporation operations on the Sellafield site, none exist for the buffer storage plant. The general approach to modelling in academia involves the generation of complex CFD models, which require expensive computational power and long simulation times. By contrast, there is a need for the development of relatively simplified and accurate models requiring little computational power and is the focus of investigation in this paper.

The HAR is an effluent stream consisting of concentrated acid with dissolved fission products and has self-heating properties. The basis for safe operation of the BSTs is to control the temperature of the contents below the bubble point of 95°C to avoid potential release of toxic vapours into the atmosphere. Whilst the primary reason for temperature control is to prevent generating radioactive vapor, there is also a secondary reason to control temperature below a certain temperature to avoid accelerating equipment corrosion rates (Grosse, 2012; Cattant *et al.*, 2008). The BSTs at Sellafield currently fulfill a purpose different to the intended design. Previous plant data from the BSTs is not useful for the new operational use. Presently it is assumed the BSTs operate adiabatically and so the prediction of a temperature response is considerably faster than that experienced on the plant. Hence, there is an urgent requirement to improve the current predictions by using a simplified and relatively accurate heat transfer model for the prediction of the temperature response of the BSTs. This will allow more efficient

operation of the buffer storage plant and save operations staff time and resources. Therefore, this discourse presents a heat transfer model that provides the prediction of the temperature response of the contents of BSTs containing HAR at Sellafield without relying on complex CFD simulations.

2. MODEL PARAMETERS

2.1 BST Dimensions

Sellafield Ltd have provided details on the dimensions and details of a single BST vessel, cooling coils and cell to allow development of a thermal model.

There are six 1200 m³ BSTs, each weighing approximately 52 tonnes empty. A full batch of liquor increases this by approximately 1200 tonnes. Each tank is constructed from 304L stainless steel with a thickness of 9.50 mm, outer diameter of 13.72 m and height of 9.14 m. All the tanks had been fitted with two 304L stainless steel steam coils for in-tank evaporation, however, evaporation procedures are now no longer carried out and these coils have since been converted to cooling coils. An additional 304L stainless steel helical cooling coil has also now been installed which traverses the tank periphery (5 turns, 1.52 m per turn). The tanks are un-jacketed. The dimensional details of the coils are listed in Table 1.

Table 1 Cooling coils details and dimensions.

Cooling Coil Details		
	Helical Cooling Coil (50 mm NB)	Base Cooling Coils (2 sets per Tank) (80 mm NB)
Coil Tube Outside Diameter (m)	0.06144	0.08766
Coil Tube Thickness (m)	0.00447	0.00488
Coil Tube Inside Diameter (m)	0.0525	0.0779
Total Length of Coils (m)	216.69	79.09
Cooling Water Flow (normal ops) (m ³ /h)	0.5	0.5

Each tank is located inside its own separate cell which has an internal cuboid structure of 15.24 m x 15.24 m x 10.97 m and external structure of 17.38 m x 17.38 m x 13.11 m. The cell is constructed from concrete and has a wall thickness of 2.14 m to provide shielding from the radioactive contents of the BST.

2.2 Thermophysical Properties

The relevant thermophysical properties used in the model have been evaluated at standard temperatures and pressure, and it is assumed that they remain independent of temperature, within the

operational range studied. The key thermophysical properties used in the model are presented in table 2.

Table 2 Thermophysical properties of the HAR, air and stainless steel used in the model evaluated at standard temperature and pressure.

	HAL (40 °C) (3 M Nitric Acid with Heating Element)	Air (25 °C)	304L Stainless Steel	
Dynamic Viscosity, μ	0.0006	1.84E-05	-	kg/ms
Density, ρ	1090.00	1.17	-	kg/m ³
Specific Heat Capacity, Cp	3480.00	1006.96	-	J/kgK
Thermal Conductivity, k	0.26	0.03	16.00	W/mK
Kinematic Viscosity, ν	5.66E-07	1.57E-05	-	m ² /s
Thermal Diffusivity, α	1.51E-07	2.22E-06	-	m ² /s
Thermal Expansivity β	4.00E-04	0.003	-	1/K

Due to the radioactive nature of the HAR material, the thermophysical properties remain unknown. In the absence of this data, it has been assumed that the HAR behaves as 3M concentrated nitric acid.

3. MODELLING HEAT TRANSFER IN THE BST BY AN ENERGY BALANCE

The model presented herein has been derived from first principles by performing an energy balance across a single BST. Fig. 2 is a schematic of the various heat flows occurring within the BST. There is a single flow of energy which leads to the generation of heat. This is the heat generated from the decaying of fission products which have been dissolved in the HAR mixture. This single heat flow is indicated by the red arrow in Fig. 2. There are 3 separate flows through which heat is removed. These include: heat loss through the 3 sets of cooling coils, heat loss through the mechanical cooling vent and natural heat losses to the surroundings (natural heat losses are modelled as losses by 2 separate avenues; losses from the liquid space and losses from the ullage space).

Heat generated within the BST, \dot{Q}_{HAR} , occurs due to the presence of decaying radioactive isotopes dissolved in the HAR mixture, as stated. Within the industry, this heat is characterised by assigning the material with a heat rating value that depends on the origin, the type of isotopes present and the age of the liquor. This rating, \dot{q}_{HAR} , is a specific quantity of heat generated per unit volume and, for standard HAR reprocessed from THORP, the heat rating is 235 W/m³.

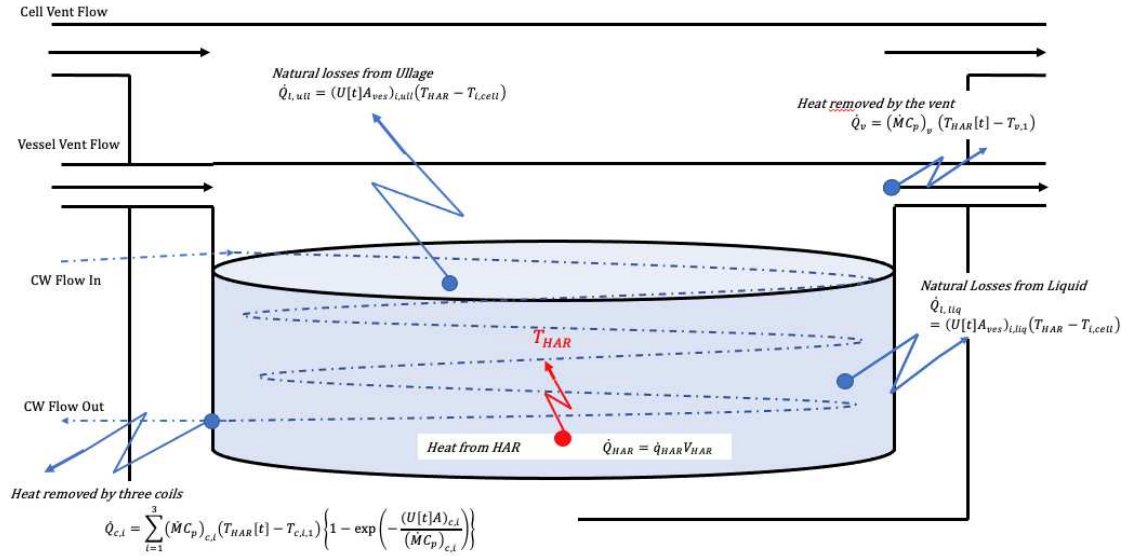


Figure 2. Schematic highlighting the contributing terms to the energy balance over a single BST.

Hence, the time variation of the temperature of the HAR depends upon a number of listed parameters:

- The heat generated from the volume of HAR V_{HAR} deposited in the BST
- The thermal inertia of the quantity of HAR in the vessel and that of the vessel and coils $\left[(\rho VC_p)_{HAR} + (\rho VC_p)_{steel} \right]$
- The flow and inlet temperature of water travelling through the cooling coils.
- The flow and inlet temperature of air traveling through the mechanical cooling vent.
- The thermal resistances for the natural heat loss and temperature of the ambient air .

The following expression Eq. (1) represents the response of the HAR temperature, $T_{HAR}[t]$, within the vessel due to the heat evolved, $\dot{q}_{HAR}V_{HAR}$, minus the summation of the enthalpy losses depicted in Fig. 2 (energy balance):

$$\left[(\rho VC_p)_{HAR} + (\rho VC_p)_{steel} \right] \frac{dT_{HAR}[t]}{dt} = \dot{q}_{HAR}V_{HAR} - \sum_{i=1}^3 (\dot{M}C_p)_{c,i} (T_{HAR}[t] - T_{c,i,1}) E_{c,i}[t] - (\dot{M}C_p)_v (T_{HAR}[t] - T_{v,1}) - \left([U_l[t] \cdot A_{l,ves}]_{liq} + [U_l[t] \cdot A_{l,ves}]_{ull} \right) (T_{HAR} - T_{l,cell}) \quad (1)$$

With initial conditions:

$$\text{For } t \leq 0, T_{HAR} = T_{HAR,0}$$

$$\text{For } t \geq 0, V = \text{constant} = V_{HAR}$$

Here, the volume of HAR is V_{HAR} , while $E_{c,i}[t]$ are the thermal effectiveness values obtained from the relationship, $E_{c,i}[t] = 1 - \exp\left(-\left(U[t]A/\dot{M}C_p\right)_{c,i}\right)$. Additionally, $U_{c,i}[t]$ are the Overall Heat Transfer Coefficients (OHTCs), $A_{c,i}$ are inner surface areas of the three cooling coils, while $\dot{M}_{c,i}$ are the mass flows and $C_{p,c,i}$ are the specific heats of the cooling water respectively. The last two terms on the right-hand side of the equation are the heat losses by the vent gas flow and those combined from the vessel liquor and ullage volumes to the cell vent gas respectively.

Note, all of the OHTCs in Eq. (1) are time dependent, due to various individual film heat transfer coefficients being dependent upon non-linear temperature differences. This creates a non-linear expression overall with respect to the temperature $T_{HAR}[t]$. In addition, this expression includes the impact of the thermal inertia of the steel contents of the BST; as adopted in the work of Johnson *et al.* (2021).

The largest contribution to heat losses is due to the 3 cooling coils in the vessel, $\dot{Q}_{c,i}$, and is around 85% of the total (see Fig 8c.). The OHTCs $U[t]_{c,i}$ for the coiling coils, based on the outside surface area of each coil ($2\pi d_{o,c,i}L_{c,i}$), are obtained from following expression:

$$\frac{1}{U[t]_{o,c,i}} = \frac{1}{h[t]_{o,c,i}} + \frac{d_{o,c,i} \ln\left\{\frac{d_{o,c,i}}{d_{i,c,i}}\right\}}{2k_{w,c,i}} + \frac{d_{o,c,i}}{d_{i,c,i}h_{i,c,i}} \quad (2)$$

The time dependency emanates from the outside film heat transfer coefficient $h[t]_{o,c,i}$ of the coils in Eq. (2), because the value at any point in time depends upon the difference between the HAR $T_{HAR}[t]$ and the outside coil surface $T_{o,c,i}$ temperatures. This coefficient is calculated from the turbulent free convection correlation provided by Eq. (3a) as follows:

$$h[t]_{o,c,i} = 0.1 \times (\text{GrPr})^{\frac{1}{3}} = 0.1 \times \left(g\beta(T_{HAR}[t] - T_{o,c,i})/(v\alpha)^2\right)^{1/3} \quad (3a)$$

(Incropera, 2007)

The other two terms in Eq. (2) represent the conduction across the wall of the coil and the forced convection coefficient, $h_{i,c,i}$, of the cooling water flow within the coil. The forced convection coefficient is calculated using the forced convection in pipes correlation provided by Incropera (2007), Eq (3b):

$$\text{Nu} = \frac{h_{i,c,i} d_{o,c,i}}{k_{c,i}} = 0.023 \text{Re}^{0.8} \text{Pr}^{\frac{1}{3}} \quad (3b)$$

3.1 Modelling Natural Heat Losses

The BST also suffers natural heat losses to the surroundings from the HAR in the vessel and the ullage region above the HAR. Far more complex expressions are required due to the multiple heat transfer mechanisms occurring both in parallel and series. These are highlighted by the resistance network in Fig. 3.

Within the liquid HAR, the heat transfer occurs by free convection currents. However, in the ullage region, heat transfers by dropwise condensation of the vapours from the vent gases, which are saturated at the same temperature as the HAR. The amount of condensation is assumed equivalent to the evaporation from the HAR surface. Having travelled from within the liquor or from the vapor in the ullage, the heat flow then transfers by conduction through the wall of the BST. At the outside wall of the vessel the heat transfer mechanism is by free convection to the cell vent gas, and also, by radiation to the inside cell wall. Then, there is next a further transfer of heat by free convection at the inside surface of the cell from the bulk cell vent gas. Heat transfer by free convection at the outside vessel wall and free convection at the inside cell wall occur in series relative to one another but both transfer mechanisms occur in parallel to the transfer of heat by radiation from the outside vessel wall to the inside cell wall (indicated in Fig 3.). The thick concrete cell wall then provides an additional resistance to heat flow. Following this, heat flows from the outside surface of the cell by free convection and radiation in parallel to the ambient surroundings.

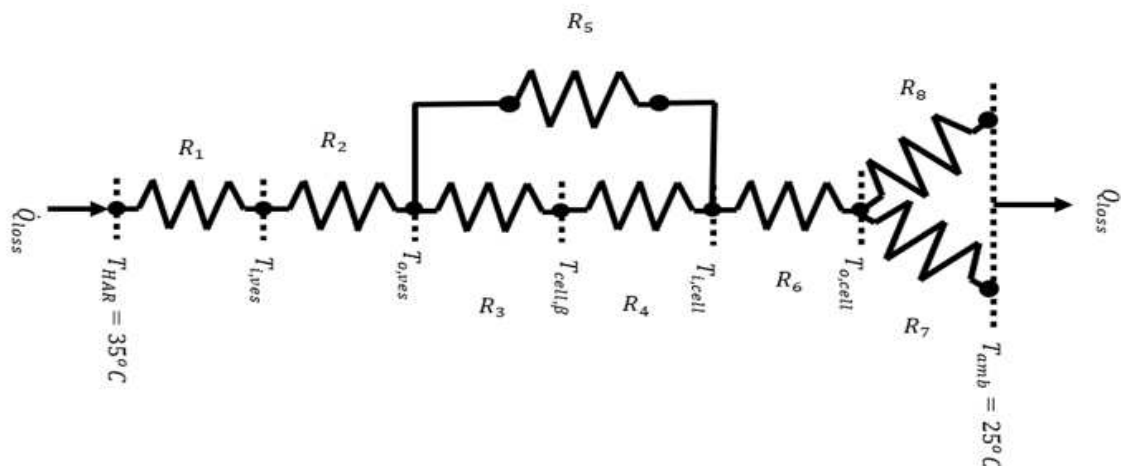


Figure 3. Resistance network for the natural heat losses from the BST to the surroundings.

The network presented in Fig 3. can be summarised as a system of 8 resistances in total with 2 of the radiation resistances occurring in parallel. Fig 3. can be represented as a system of 6 equations with 6 unknowns (as shown in Eqs. (4)-(9)).

$$\frac{\dot{Q}_{loss}}{A_{I,ves}} = h_{I,ves}(T_{HAR} - T_{I,ves}) \quad (4)$$

$$\frac{\dot{Q}_{loss}}{A_{I,ves}} = \frac{2k_{w,ves}}{d_{I,ves} \ln \left\{ \frac{d_{O,ves}}{d_{I,ves}} \right\}} (T_{I,ves} - T_{O,ves}) \quad (5)$$

$$\frac{\dot{Q}_{loss}}{A_{O,ves}} = h_{O,ves}(T_{O,ves} - T_{cell,\beta}) + h_{O,ves,r}(T_{O,ves} - T_{I,cell}) \quad (6)$$

$$\dot{Q}_{loss} = h_{I,cell}A_{I,cell}(T_{cell,\beta} - T_{I,cell}) + h_{O,ves,r}A_{O,ves}(T_{O,ves} - T_{I,cell}) \quad (7)$$

$$\frac{\dot{Q}_{loss}}{A_{I,cell}} = \frac{k_{w,cell}(L_1H_2 - H_1L_2)}{\delta \ln \left\{ \frac{L_1H_2}{H_1L_2} \right\}} (T_{I,cell} - T_{O,cell}) \quad (8)$$

$$\frac{\dot{Q}_{loss}}{A_{O,cell}} = (h_{O,cell} + h_{O,cell,r})(T_{O,cell} - T_{amb}) \quad (9)$$

The free convection film coefficient inside the vessel, $h_{I,ves}$, is dependent upon the temperature difference between the HAR liquor and the inner vessel surface, and the free convection coefficients, $h_{O,ves}$ and $h_{I,cell}$, depend upon differences between the outer vessel surface and the bulk cell temperatures, and between the bulk cell and the inner cell surface temperatures respectively. Additionally, $h_{O,cell}$ is dependent on the temperature difference between the outside surface temperature of the cell and the ambient temperature of the surroundings. These coefficients are obtained using an identical correlation to that presented in Eq (3) but using the relevant properties depending upon the fluid through which heat is being transferred.

The radiation heat transfer coefficients, $h_{O,ves,r}$ and $h_{O,cell,r}$, have been calculated based on the correlation provided in Eq (10) and Eq (11) respectively.

$$h_{O,ves,r} = \sigma \left(\frac{1}{\varepsilon_{ves}} + \frac{A_{ves}}{A_{cell}} \left\{ \frac{1}{\varepsilon_{cell}} - 1 \right\} \right)^{-1} \left(\frac{T_{O,ves}^4 - T_{I,cell}^4}{T_{O,ves} - T_{I,cell}} \right) \quad (10)$$

$$h_{O,cell_r} = \varepsilon_{cell}\sigma \left(\frac{T_{O,cell}^4 - T_{amb}^4}{T_{O,cell} - T_{amb}} \right) \quad (11)$$

Each of Eqs (4)-(9) is highly non-linear with respect to temperature differences, making solution very difficult. A numerical solution procedure has been undertaken to simultaneously solve this system of equations using built-in Microsoft Excel® GOALSEEK™ algorithms. The solution technique is best represented by the logic flow diagram provided in Fig 4. The method outlined by figure has been developed using precedence ordering techniques as deployed in the work of Hegg and Walton (1998).

The results from a full solution to the system of Eqs (4)-(9), for a range of T_{HAR} , is presented within the Electronic Supplementary Materials (ESM) in table S1 and Fig. S1.

The solution to the system of Eqs (4)-(9) indicates that the resistance to heat transfer across the network (Fig 3.) is completely dominated by the conduction resistance of the concrete walls of the cell, which are approximately 2 metres thick. This is indicated by the large drop in temperature across the cell wall (see data in ESM table S1) compared with the temperature drop across the other heat transfer resistances. Hence, the cell can be considered to act adiabatically, that is, a perfect insulating material. Therefore, in order to avoid an excessively pessimistic approach, the overall resistance network illustrated in Figure 3 is only evaluated up to the inner cell wall temperature, $T_{I,cell}$, to capture the heat losses from the liquid contents of the BST to the inside surface of the cell wall. $T_{I,cell}$ has then been evaluated using the correlation depicted in Eq (12) which was developed from the solution to the full problem (see the data presented in Fig. S2 of the ESM).

$$T_{I,cell} = (0.75 \cdot T_{HAR}) + 75.55 \quad (12)$$

The OHTC $U_{l,liq}[t]$ in Eq. (1), is based on the inside surface area, $(A_{l,ves})_{liq}$, of the vessel in contact with the HAR liquor and is evaluated by the expression detailed in Eq. (13), which contains individual film coefficients for free convection and radiation.

The OHTC $U_{l,ull}[t]$ in Eq.(1), is based upon the inside surface area of the ullage region, $(A_{l,ves})_{ull}$, and is obtained from an identical expression to Eq. (13). The only difference being the evaluation of the heat transfer coefficient for the inside vessel surface. During calculation of $U_{l,ull}[t]$, the heat transfer coefficient for the inside vessel surface is evaluated using a dropwise condensation correlation provided by Rose (1994) (Eq. (14)) which depends upon the difference between the temperature of the saturated gas in the ullage volume and the inner vessel surface temperature.

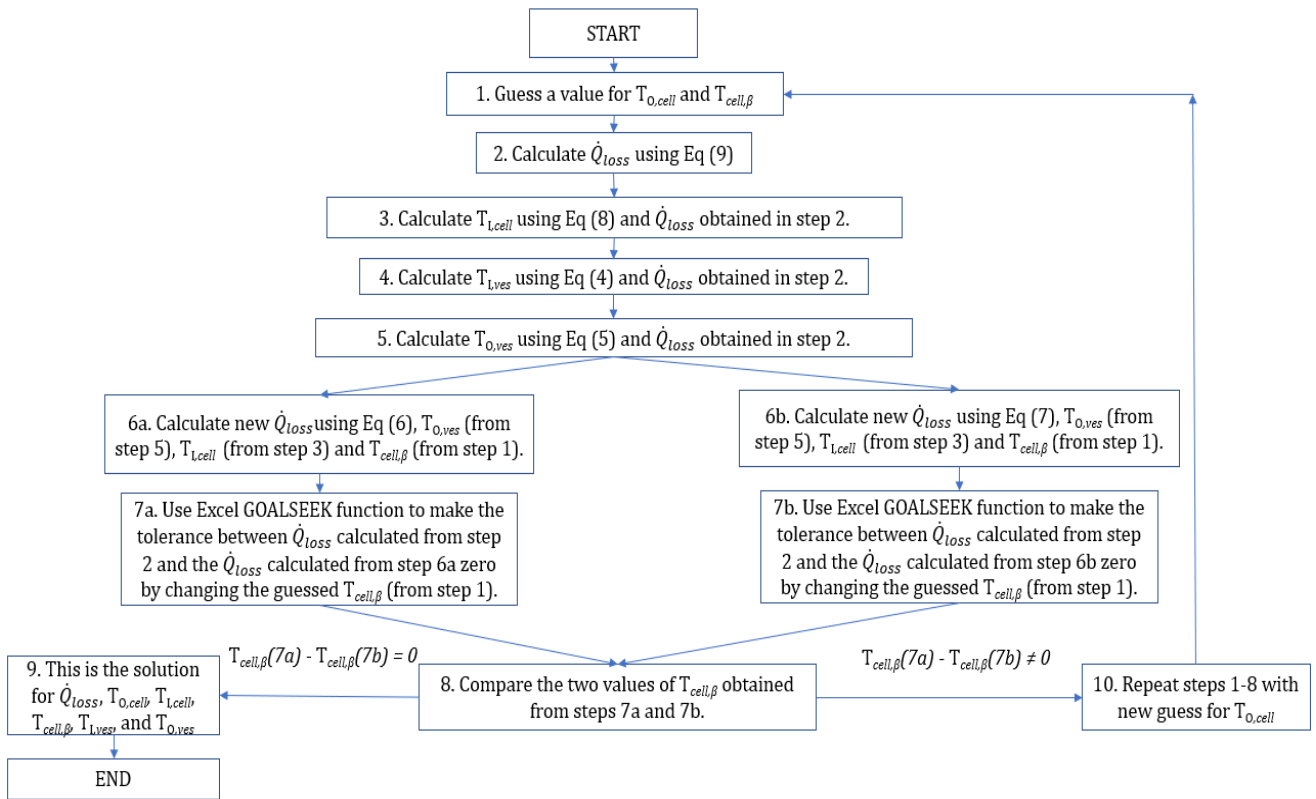


Figure 4. Logic flow diagram demonstrating the method used to solve the simultaneous set of non-linear equations (4)-(9).

$$h_{1,ves} = T'_{HAR}{}^{0.8} (5 + 0.3\{T_{HAR} - T_{1,ves}\}) \quad (14)$$

$$\frac{1}{U_{l,liq}} = \frac{1}{h_{1,ves}} + \frac{d_{1,ves} \ln\left\{\frac{d_{0,ves}}{d_{1,ves}}\right\}}{2\pi k_{w,ves}} + \frac{A_{l,liq,ves}}{\left[(h_{1,cell} A_{1,cell}) + \frac{1}{\left(\frac{1}{h_{0,ves} A_{0,ves}} + \frac{1}{h_{0,ves,r} A_{0,ves}} \right)} \right]} \quad (13)$$

The time variations of the values of $U_{l,liq}[t]$ and $U_{l,ul}[t]$ emanate from the varying HAR temperatures, which causes all the film coefficients and all surface temperatures to also vary with time. Hence, the evaluation of all these coefficients requires a solution to sets of simultaneous non-linear algebraic equations (Eq (4)-(9)) which represent the heat flow from the vessel to the surroundings. The residence time of the vent gases in the cell is a matter of hours and so it is assumed that the temperature is uniform throughout the cell.

3.2 Model Assumptions

The assumptions associated with the model are outlined as follows:

- 1-dimensional conduction of heat flow. Whilst modelling in 2 or potentially 3 dimensions could have more accurately reflect the actual temperature response in the BST, this would have added significant complexity to the model with seriously increasing the computational requirements. The aim of this research is to develop a simplified heat transfer model that is used provide trends in how temperature will vary as a function of some key parameters, therefore it is considered satisfactory to assume 1-dimensional conduction of heat flow to avoid development of a complex CFD model
- The thermophysical properties are independent of temperature., Some of thermophysical properties in reality will vary with temperature to some degree. However again, maintaining the idea that the model developed is a simplified approach, it is concluded that the variation in thermophysical properties with temperature is not warranted and will not have a significant impact on predictions. This is further confirmed by the validation results depicted in Fig. 6 (b).
- The thermophysical properties of HAR assumed to be equal to 3M concentrated nitric acid.
- The HAR is well mixed and so the temperature is the same everywhere in the vessel. This assumption may not entirely reflect what happens in reality. During this research the authors speculated that the existence of a temperature gradient within the vessel may be a more likely occurrence. It is anticipated that, because the vessel cooling coils run along the bottom of the vessel, and also, traverse the tank periphery, the contents of the vessel are likely to exhibit the effects of a reverse unconstrained thermosyphon situation. Panesar (2016) revealed by a CFD simulation that an unconstrained thermosyphon occurs in the evaporators at Sellafield, which leads to are relatively small temperature variation throughout the vessel contents. However, modelling this situation for a BST would require the use of expensive and computationally intensive CFD software, which is not what the authors desire to achieve with this research. The idea behind this research is to develop a simple, low cost and fast model that can provide staff with trend predictions to make operational decisions about the plant. Investigation of the presence of temperature gradients due to a reverse unconstrained thermosyphon effect using complex CFD analysis is suggested as a potential avenue for future work in this subject area. In accordance with the aims of this research this assumption is confirmed by Fig. 6 (b).
- The vapour in the ullage region is in thermal equilibrium with the HAR. This assumption is expected to reflect reality because the vessel ventilation is low enough to assume heat transfer by free convection at the liquor surface ($Gr/Re^2 \gg 1$) (Incropera 2007).

- The heat loss from the inside surface of the ullage region is caused by dropwise condensation of water. This is justified based on the work of Rose (1994) who developed the correlation used to model condensation at the inside surface of the vessel in the ullage region.
- The condensed water flows back into the HAR and is equal to the heat lost from evaporation of water from the HAR surface. In reality this may not be case and there may further heat loss through evaporated liquor. However, previously it is assumed that the vessel vent flow is not sufficient to disrupt any thermal equilibrium between the vapour in the ullage region and the liquid HAR. To maintain consistency, it remains justified to assume that the vessel vent flow is not significant to allow any further heat losses due to evaporation. Again, this is further confirmed by the validation result depicted in Fig. 6 (b).
- The temperature throughout the cell is uniform. This is considered a reasonable assumption, because the cell vent flow is low through a large cell volume and with a significant residence time of **xxx mins** so that the air is effectively stagnant and heat transfer is by free convection.
- The concrete cell wall acts as a perfect insulator. Table S.1, Fig S.1 and Fig S.2 present the results from solution to the full natural heat loss problem. These results indicate a significant drop in temperature across the cell wall (see data in ESM table S1) compared with the temperature drop across the other heat transfer resistances. Hence, the cell can be considered to act adiabatically, that is, a perfect insulating material. Therefore, it is assumed there is no further heat loss beyond the cell wall and the overall resistance network presented in Fig. 3 is only evaluated up to the inside cell wall during evaluation of the OHTC for natural heat loss. This means the inner cell surface temperature must be known to allow the OHTC for heat loss to the surroundings to be evaluated. The temperature of cell inner surface is related to the temperature of the HAR as indicated by Eq (12). Eq 12 has been developed from the data presented in the Fig. S2 of ESM.

3.3 Solution methodology

A numerical solution of Eq. (1) provides a prediction for the temperature response of the contents of the BST. Having established an appropriate time interval, it is possible to numerically determine the change in the temperature of the BST contents, using Euler's approximation formula, Eq. (15).

$$T_{HAR}[t_{n+1}] = T_{HAR}[t_n] + \frac{dT_{HAR}}{dt} \times \Delta t \quad (15)$$

The solution procedure adopted to solve Eq (1) using Euler's approximation formula can be summarized by Fig 5. Note that this figure makes reference to the flow logic diagram depicted in Fig 4; that is, the flow diagram presented in Fig 4 is embedded within the flow diagram displayed in Fig 5.

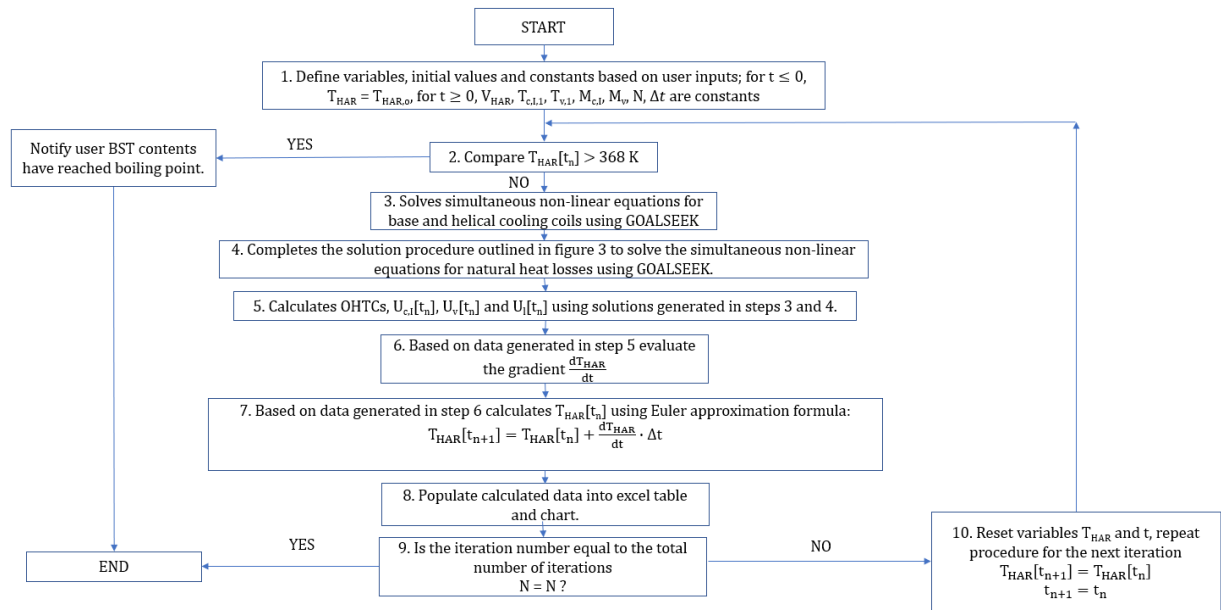


Fig 5. Logic flow diagram demonstrating the method used to solve the non-linear ODE, Eq. (1).

The temperature profile generated from the Euler approximation is first order accurate with the size of the step. In order to be confident of convergence, a predictor-corrector numerical solution procedure is also used - the trapezoidal formulation, Eq. (16). Provided the results from Euler's approximation are within the tolerance specified for the trapezoidal predictor-corrector (TPC) technique, convergence can be assumed.

$$T_{HAR}[t_{n+1}] = T_{HAR}[t_n] + \left(\left. \frac{dT_{HAR}}{dt} \right|_n + \left. \frac{dT_{HAR}}{dt} \right|_{n+1} \right) \times \frac{\Delta t}{2} \quad (16)$$

Both numerical solutions require iterations for each time step due the evaluations of the OHTCs and the various film heat transfer coefficients. These sets of equations are re-arranged by the precedence ordering technique to facilitate robust solution algorithms for each OHTC. The predictions by both techniques have been developed as a VBA code for solution in Microsoft Excel®. An example screenshot of the Excel® model interface is presented within the ESM (Fig. S3).

4. RESULTS & DISCUSSION

Table 3 provides a summary of the computational experiments that have been undertaken and discussed as part of this research. In this study, the convergence of the Euler solution is investigated by comparison with a solution using the trapezoidal predictor-corrector technique. This highlights whether the time step being used is small enough to obtain a converged solution. This was achieved by running identical simulations, but using different solution techniques once via Euler's approximation and once via the trapezoidal predictor-corrector technique. Fig. 6 (a) presents the temperature response prediction from simulation of a full tank of HAR with a heat rating of 235 W/m³. The cooling water flow to all the

coils is 0.5 m³/h per coil. Fig. 6 (a) confirms convergence has been achieved; both plots almost directly overlap one another. The proposed model predicts that, under the conditions outlined above the tank's contents will reach a temperature of approximately 70°C over the course of approximately 30 days regardless of the solution procedure (Euler, trapezoidal) adopted. The conclusions drawn from Fig. 6 (a) highlight that Euler's approximation, using a time step, $\Delta t = 5000$ s, provides an adequate converged

Table 3 Summary of computational experiments and simulations undertaken in this research. For each experiment the volume, heat loading, cooling water flow and vessel vent status are defined.

<i>Computational Experiment Title</i>	<i>Run No.</i>	<i>BST contents Volume (m³)</i>	<i>HAR Heat Rating (W/m³)</i>	<i>Cooling Water Flow (m³/h per coil)</i>	<i>Vessel Vent (ON/OFF)</i>	<i>Numerical Solution Procedure</i>
<i>Investigation for Convergence</i>	1a	1171 (full tank)	235	0.5	ON	Euler
	1b	1171	235	0.5	ON	TPC
<i>Validation with Plant Data</i>	2	810	70	0.5	ON	Euler
<i>Varying volume upon loss of cooling and loss of vent supply</i>	3. a	200	235	0	ON	Euler
	3. b	400	235	0	ON	Euler
	3. c	600	235	0	ON	Euler
	3. d	800	235	0	ON	Euler
	3. e	1000	235	0	ON	Euler
	3. f	1171	235	0	ON	Euler
	3. g	1171	235	0	OFF	Euler
<i>Misroute of HAL</i>	4	1171	3500	0.5	ON	Euler
<i>Varied Cooling Water Flow</i>	5. a	1171	235	0	OFF	Euler
	5. b	1171	235	0.3	OFF	Euler
	5. c	1171	235	0.6	OFF	Euler
	5. d	1171	235	0.9	OFF	Euler
	5. e	1171	235	1.2	OFF	Euler
<i>Comparing Proposed Model with current approach</i>	6. a	1171	235	0.5	ON	Euler
	6. b	1171	3500	0.5	ON	Euler

solution of sufficient accuracy. Therefore, this justifies use of Euler's solution technique and there is no requirement to investigate solution convergence by reducing the time step. Future simulations are computed using Euler's method with time step, $\Delta t = 5000$ s.

Fig. 6 (b) presents predictions of measured site data from an actual large-scale BST containing 810 m^3 of HAR material with a heat rating at 70 W/m^3 and with an equilibrium temperature of 23.4°C , which is slightly lower than the measured equilibrium temperature of 22.5°C . This model overprediction provides an acceptable conservative projection, without the recourse of adopting expensive CFD simulations. It is also noted that there is a considerable level of scatter within the tank temperature measurements (although both model prediction and experimental data are within acceptable levels of variation). Fig. 6 (c) provides the temperature response predictions for varying volumes of HAR with loss of the cooling water supply for a HAR rating of 235 W/m^3 . A HAR volume of approximately 200 m^3 will barely the change temperature. However, with increasing volumes, higher equilibrium temperatures occur and the highest is around 87°C for a volume of 1171 m^3 . Such predictions highlight the powerful advantage of using simplified 1D models for analysis. These predictions are computationally easy to complete and will give plant operators important insight into expected temperature variations as fill levels vary, leading to safe low-risk operations.

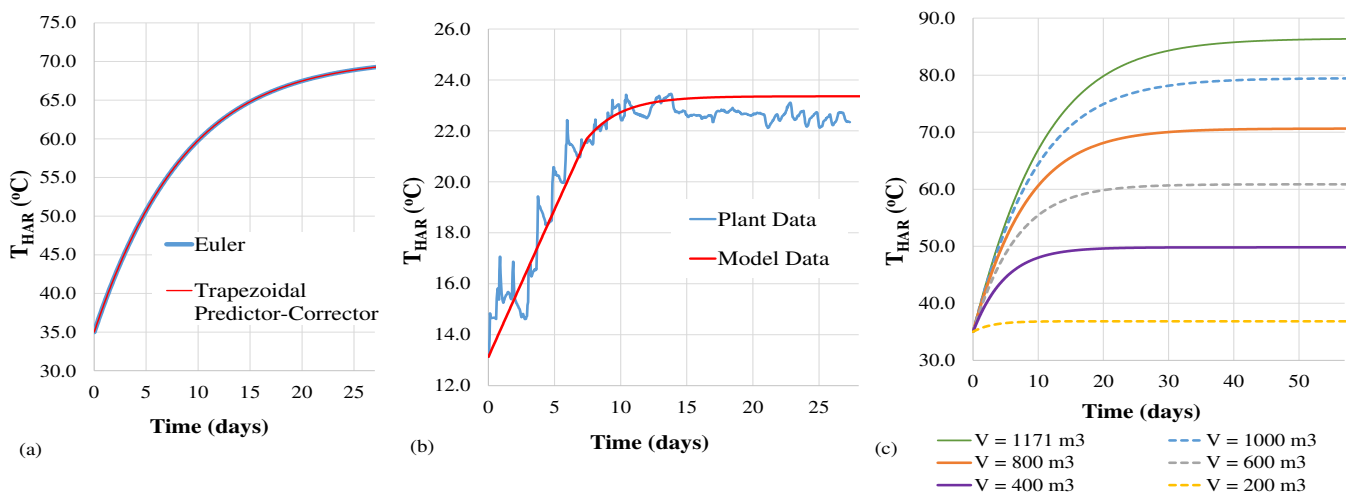


Figure 6. (a) Temperature-time profiles for a full tank of HAR rated at 235 W/m^3 by both solutions at a Δt of 5000 s. (b) Temperature-time profiles from measured real plant data and model predictions. (c) Temperature-time predicted profiles for varying HAR volumes and loss of cooling water flow at a heat rating of 235 W/m^3 . Colour required for this figure.

The current approach to operations on the Sellafield site is to use the zero-heat loss (ZHL) method, which results in a linear temperature-time relationship (Sellafield Ltd 2020). Fig. 7 (a) is a plot of temperature responses by the ZHL and model predictions for a full tank of HAR rated at 235 W/m^3 with the cooling water flow active at $0.5 \text{ m}^3/\text{h}$ per coil and with the vessel and cell vent flows active. The

linearity of the ZHL relationship diminishes when allowing for heat losses and reveals the significant conservation associated with the ZHL assumption. The bubble point of 95°C is reached after approximately 11 days by the ZHL approach, whereas the model prediction reaches an equilibrium temperature of 70.4°C after approximately 35 days. A further operational parameter is the ejector strike temperature, which is 67°C. The ejector strike temperature is the maximum temperature the motive fluid (steam) can reach in an ejector device. If steam exceeds this temperature this causes low motive flow and a phenomenon known as breaking the shockwave (striking) occurs. This deteriorates the ejector performance and can lead to wastage of steam and reduction in operation efficiency.

The ZHL method predicts that the ejector strike temperature will be reached in approximately 6 days. However, the proposed model predicts over double this time (67% longer, approximately 15 days). Therefore, it appears that the current linear ZHL approach can be significantly overconservative, in terms of predicted temperature rises. While, such conservatism is clearly beneficial from a standpoint of risk, the improved modelling with the current approach will allow for a larger envelope of operational conditions and will reduce costs. Also plotted in Fig. 7 (a) are the predictions of the cascade of temperatures through the BST system with time; the outside surface of the vessel, the bulk cell and the inside of the cell temperatures. These data cannot be predicted by the fundamental ZHL approach, evidencing the greater predictive function of the new model.

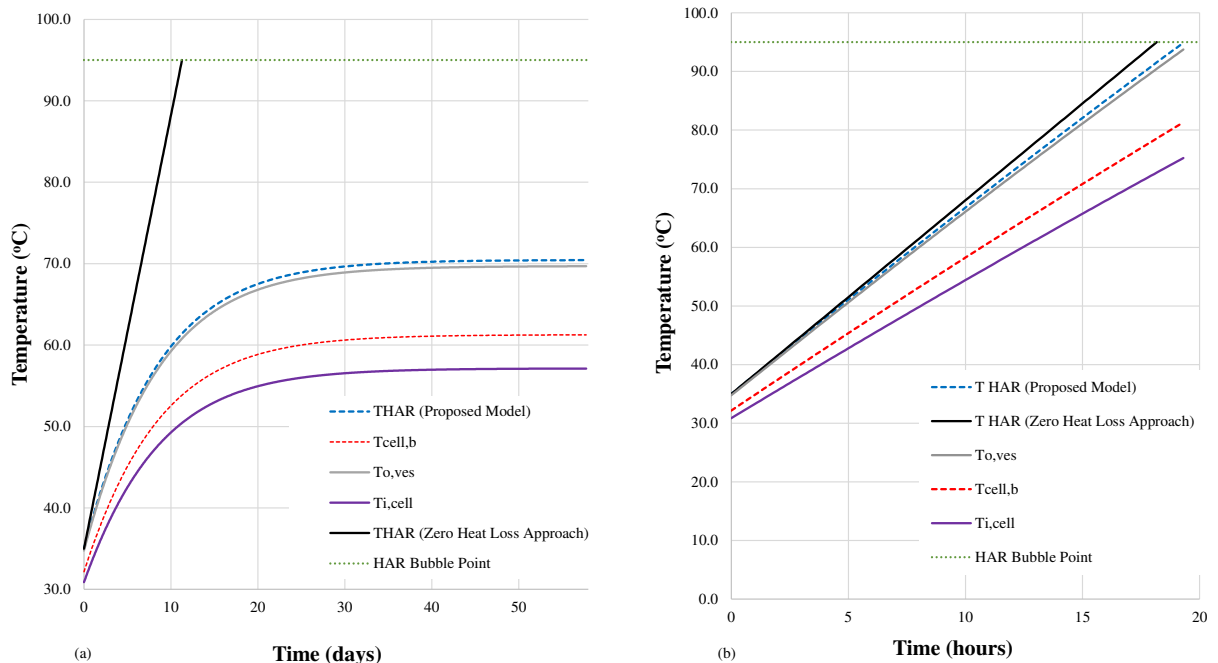


Figure 7 (a) Temperature-time plots predicted by the proposed model and the ZHL approach used in current operations. b) Plots predicted at higher heat loading by both ZHL and the model. Colour required for this figure.

Fig. 7 (b) is a plot of temperatures for a full BST of 1171 m³ of HAR, a heating rate of 3500 W/m³ and a cooling water flow of 0.5 m³/h per coil with both vent and cell flows activated. At this higher heat loading, the temperature-time plot predicted by the proposed model exhibits linearity and follows closely the ZHL profile. The similarity in predictions is caused by the heat released by the HAR being orders of magnitude larger than the amount removed by the various heat losses. At lower heat loadings, the difference in magnitude between the heat generated by the HAR and the heat removal is not so large and the ZHL is no longer valid. In summary, it becomes clear that at low to medium heat loadings of HAR, the proposed model provides a useful predictor of the temperature response behaviour of the contents of the BST. In addition, the ZHL approach fails to provide details of intermediate temperatures, Q-values and overall heat transfer coefficients, which can all be extracted from the output of the proposed model.

The cooling impact from the coils in a full tank of HAR rated at 235 W/m³ was assessed by simulations with varied cooling water flows. Fig. 8(a) presents the predicted temperature response for various cooling water flows. In each simulation, the vessel vent status was switched to “OFF” to isolate the impact of the coils. Observation of Fig. 8(a) highlights that, as the cooling water flow increases the impact of the cooling coils becomes less marked. In other words, as the flow is raised the reduction in equilibrium temperature that is reached becomes smaller. This change can be explained by observation of the behaviour of the overall heat transfer coefficient with varying cooling water flow as projected by Fig. 8(b). Fig 8(b) indicates that, as the cooling water flow increases, the coefficient also increases, but begins to approach a constant value of around 200 W/m² K. This behaviour limits the heat that can be removed by the cooling coils, and explains the temperature responses exhibited in Fig. 8(a), which indicates there is a specific point beyond which increasing the cooling water flow will not result in any further cooling impacts.

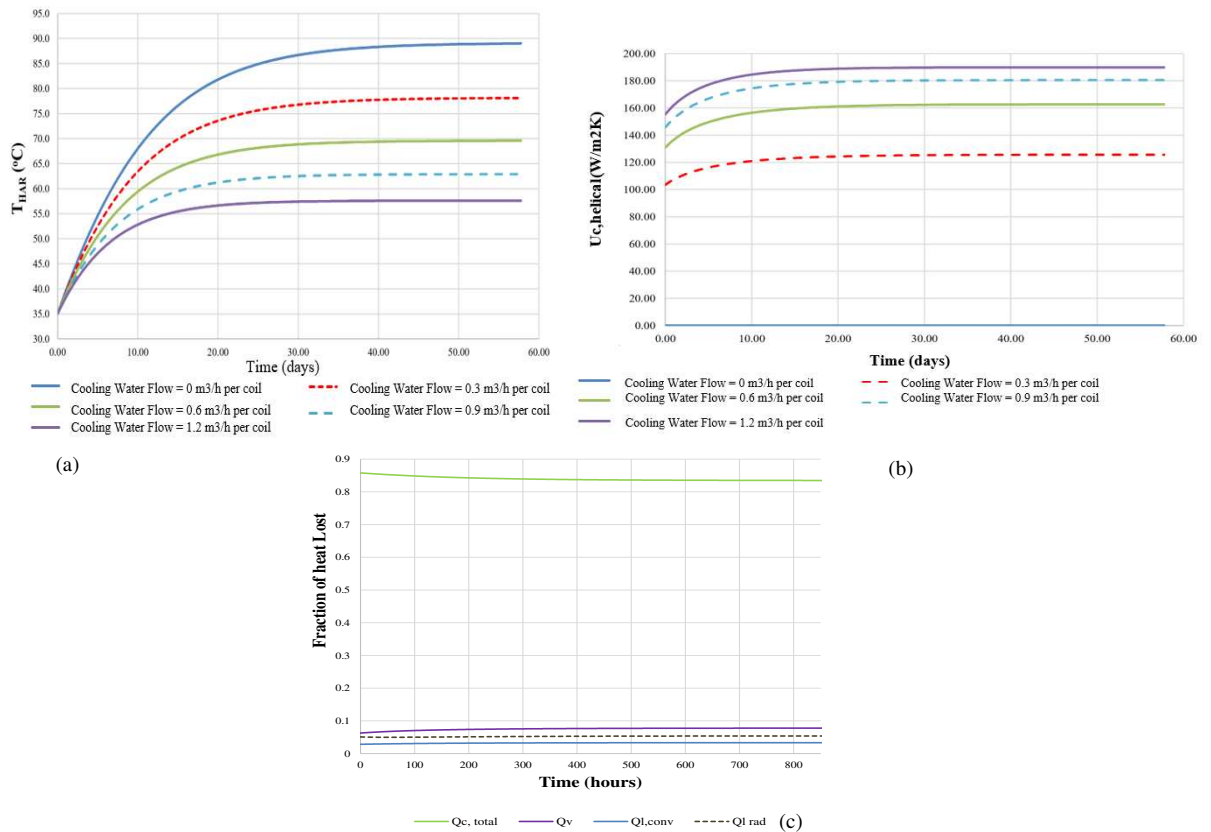


Figure 8 (a) Temperature-time plots predicted by the proposed model (b) Variation of the overall heat transfer coefficient for the helical cooling water coil with increasing cooling water flows from 0 m³/h per coil to 1.2 m³/h per coil increasing in increments of 0.3 m³/h per coil. (c) Distribution of heat via the proposed heat loss mechanisms, cooling water flow 0.5 m³/h per coil. Colour required for this figure.

The impact of the cooling coils relative to the other heat loss mechanisms is presented in Fig. 8(c), showing the distribution of heat loss via the proposed mechanisms in the BST. Fig. 8(c) indicates the major heat loss mechanism is via the cooling coils. This agrees with discussion from Turvey and Hone (2000) during safety examination of the HAST vessels, where the major contributor to heat loss mechanisms is also suggested to be through the cooling coils (when they are active). This result is to be expected because the HASTs are also designed for the purpose of storing self-heating liquor. The HASTs differ only in that they have been designed to handle post evaporative concentrated HAL with significantly higher heat loading. This reveals that the most effective method for temperature control in the BSTs is through operation of the cooling coils.

Figure 9 presents the temperature response upon combined loss of cooling water and vent supply, a critical safety concern in operation. The data indicate that in this worst-case scenario, the contents will reach an equilibrium temperature of approximately 89°C, approximately 3°C higher than is predicted if cooling water supply alone was lost. From an operational stand-point, temperatures are predicted to remain below the bubble point (95°C), but exceed the ejector strike temperature (67°C). Importantly, the simulations suggest that cooling from the vent system also has a small, but measurable, impact the temperature response of the BSTs, and therefore, it is recommended that the cooling vents continue to be considered in heat transfer assessments of the buffer tanks.

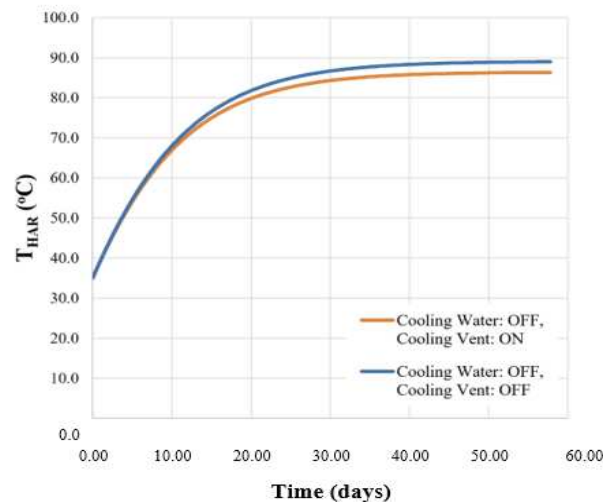


Figure 9. Temperature-time plots predicted by the proposed model with mechanical cooling vent “ON” compared to predictions when the mechanical cooling vent is turned “OFF”. Cooling water flows are turned “OFF” during both simulations. Colour required for this figure.

These findings play an important role in the wider context of nuclear engineering. Staff can use specific model simulations and results to provide more information from which they can make informed decisions around plant operations. This will lead to improved efficiency of operations; the plant operators will have a greater understanding of the length of time they safely store material in the tank without reaching temperatures outside of the operational envelope. In addition to this, the research undertaken as part of the development of this model (outlined in detail in section 3 and section 3.1) has led to an improved understanding of the physical and heat transfer phenomenon occurring in high-level nuclear waste storage processes. This contributes to the requirement for an improved understanding of nuclear legacy waste treatment mechanisms that allow safe disposal of radioactive material (Turvey and Hone 2000, Hanson 2014 and 2015).

5. CONCLUSIONS

1. A simplified heat transfer model is presented that predicts the temperature response of the contents of BSTs containing HAR at Sellafield.
2. Expressions for the non-linear overall heat transfer coefficients were derived and solved using precedence ordering techniques at each time interval (Heggs and Walton, 1998).
3. The solutions presented herein have been generated by 2 separate numerical procedures with results within $\pm 0.1\%$ of one another, which demonstrate numerical convergence.
4. Results have been demonstrated to show strong agreement with plant temperature measurements.
5. The results from the model highlight that, in certain scenarios, the BSTs can safely store material without reaching the ejector strike temperature for approximately 67% longer than is predicted by current practice (which ignores heat loss).
6. Overall, the greatest contribution to heat loss was through the sets of cooling coils (approximately 85% of total heat loss) with similar trends having been reported in other published literature.
7. The simulation results also indicated that the mechanical vent had a notable impact on cooling the BST vessels; the BSTs reached an equilibrium temperature approximately 3°C higher when the vessel vent status was switched to “OFF”.
8. The simulation run time for model described in this paper is approximately 20 minutes.
9. Non-specialist operations staff can both access and operate the model to produce results from a range of scenarios in a short amount of time. This model provides operations staff on the plant more information from which they can make more informed decisions on how to operate the facility.

ACKNOWLEDGEMENTS

Initial exposure and experience of the BST was obtained during a year placement with Sellafield Ltd (SL) by the first author. Many thanks are given to Stuart Budd and Ian Atkin of SL for their assistance and help throughout the placement, and especially to Mathew Aukett (SL systems engineer) for providing plant data.

REFERENCES

Alane, A, and Heggs, P. J. 2011. 'Experimental study of complex two-phase instabilities during the start-up of a vertical thermosyphon reboiler operating under vacuum', *Chemical Engineering Research and Design*, 89: 2012-23.

Bux J, Paul N, Peakall J, Hunter TN, Dodds J, and Biggs S. 2017. In situ characterization of mixing and sedimentation dynamics in an impinging jet ballast tank via acoustic backscatter. *AIChE Journal*, 63, 2618-2629

Ali, Muzammil, Tariq Mahmud, Peter John Heggs, and Mojtaba Ghadiri, 2020, Zonal modelling of a counter-current spray drying tower, *Chemical Engineering Research and Design*, Volume 155, Pages 180-199, ISSN 0263-8762, DOI: <https://doi.org/10.1016/j.cherd.2019.12.018>.

Barth, Nicolas. Daniel George, Frédéric Bouyer, Aurélien Schwartz, Charles-Henri Lambert, Saïd Ahzi, and Yves Rémond. 2020. 'An inverse method predicting thermal fluxes in nuclear waste glass canisters during vitrification and cooling', *Nuclear engineering and design*, 364: 110686.

Case, John B., Harris R. Greenberg, and Bruce E. Kirstein. 2020. 'Practicality of Analytical Solutions for Heat Transfer in Circular Systems in the Infinite Region to Describe Temperatures Due to Disposal of Heat-Decaying Nuclear Waste', *Nuclear Technology*: 1-12.

Cattant, François. Didier Crusset and Damien Féron. 2008. Corrosion issues in nuclear industry today. *Materials Today*. Volume 11, Issue 10. Pages 32-37. ISSN 1369-7021. DOI: [https://doi.org/10.1016/S1369-7021\(08\)70205-0](https://doi.org/10.1016/S1369-7021(08)70205-0)

Dakkoune, Amine, Lamiae Vernières-Hassimi, Dimitri Lefebvre, and Lionel Estel. 2020. 'Early detection and diagnosis of thermal runaway reactions using model-based approaches in batch reactors', *Computers & Chemical Engineering*, 140: 106908.

Grosse, M. 2012. 9 High-temperature oxidation in nuclear reactor systems. Editor(s): Damien Féron. In *Woodhead Publishing Series in Energy. Nuclear Corrosion Science and Engineering*. Woodhead Publishing. Pages 265-300. ISBN 9781845697655. DOI:<https://doi.org/10.1533/9780857095343.3.265>.

Hanson, B. C. 2014. *Nuclear fuel cycle: A UK perspective* (American Chemical Society (ACS)).

Hanson, Bruce. 2015. '6 - Process engineering and design for spent nuclear fuel reprocessing and recycling plants.' in Robin Taylor (ed.), *Reprocessing and Recycling of Spent Nuclear Fuel* (Woodhead Publishing: Oxford).

Heggs, P.J., and C. Walton. 1998. "Precedence Ordering Techniques." In Institute of Mathematics and its Applications Conference Series, 175-80. Oxford University Press.

Incropera, Frank P. 2007. Fundamentals of heat and mass transfer (Wiley: Hoboken, N.J).

Johnson, Michael, Karrar H. Al-Dirawi, Erik Bentham, Tariq Mahmud, and Peter J. Heggs. 2021. Industrial & Engineering Chemistry Research 60 (3), 1316-1325. DOI: 10.1021/acs.iecr.0c05133

Panesar, Jujar Singh. 2016. The Numerical Study of Heat Transfer and Multiphase Flows in Sub-Atmospheric Industrial Evaporators. PhD thesis, University of Leeds.

Rose, J. W. 1994. 'Dropwise Condensation ', Heat Exchanger Design Update, 2.6.5: 1-11.

Shiels J, Harbottle D, Hunter TN. 2018. Synthesis and Physical Property Characterisation of Spheroidal and Cuboidal Nuclear Waste Simulant Dispersions. Materials. 11, 1235.

Turvey, F. J., and C. Hone. 2000. "Storage of liquid high-level radioactive waste at Sellafield an examination of safety documentation." Ireland: Radiological Protection Institute of Ireland. DOI: http://inis.iaea.org/search/search.aspx?orig_q=RN:33022572.

United Nations. 2015. "Paris agreement." In Report of the Conference of the Parties to the United Nations Framework Convention on Climate Change (21st Session, 2015: Paris). Retrived December, 2017. HeinOnline.

Zhou, Xiangyun, Annan Zhou, and De'an Sun. 2020. 'Three-dimensional thermal analysis of the repository for high-level radioactive nuclear waste', International journal of energy research, 44: 8208-20.

ELECTRONIC SUPPLEMENTARY MATERIAL (ESM)

RESULTS FROM SIMULTANEOUS SOLUTION OF EQS (4) – (9) FOR A RANGE OF $T_{HAR} = 35^{\circ}C - 90^{\circ}C$.

Table S.1 – Calculated intermediate temperatures, individual and overall heat transfer coefficients from simultaneous solution of Eq (4) – (9). The solution procedure is outlined in in figure 3.

T_{HAR}	$T_{L,ves}$	$T_{O,ves}$	$T_{cell,\beta}$	$T_{I,cell}$	$T_{O,cell}$	\dot{Q}_{loss}	$h_{L,ves}$	$h_{O,ves}$	$h_{L,cell}$	$h_{O,cell}$	$h_{O,ves,r}$	$h_{O,cell,r}$	U_{loss}
°C						kW	$\frac{W}{m^2 \cdot K}$						
90.0	88.0	87.9	76.9	72.0	30.1	79.7	117.110	5.693	4.372	4.427	8.801	5.790	0.321
70.0	68.5	68.4	60.1	56.4	28.6	52.9	105.712	5.193	3.988	3.932	7.554	5.745	0.318
50.0	49.1	49.0	43.9	41.6	27.0	27.8	89.987	4.416	3.390	3.255	6.457	5.700	0.313
35.0	34.6	34.6	32.3	31.3	25.8	10.4	70.314	3.360	2.582	2.424	5.729	5.666	0.304

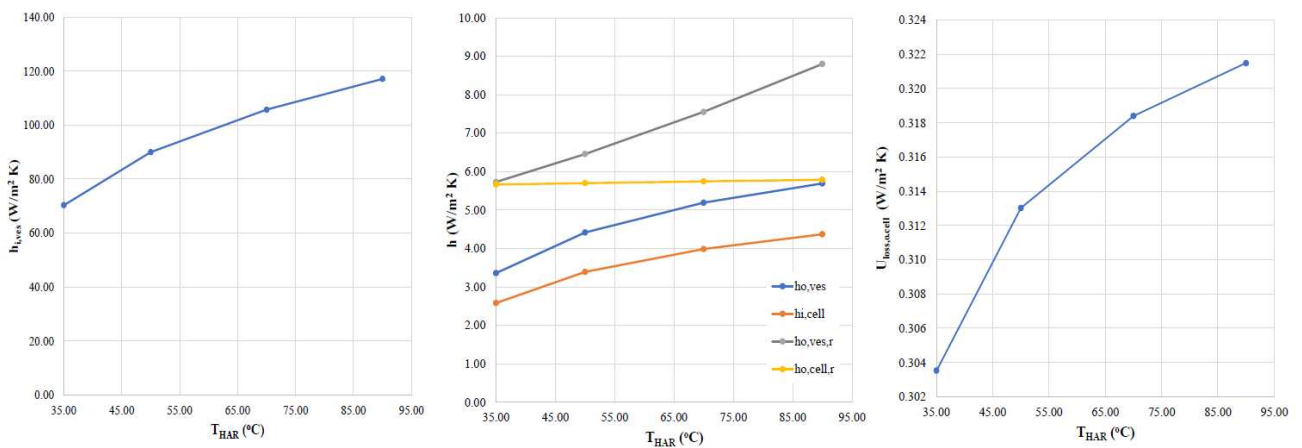


Figure S.1 – Plots of (a) inside vessel heat transfer coefficient (b) outside vessel, inside cell, outside vessel radiative and outside cell radiative heat transfer coefficient (c) Overall natural heat loss heat transfer coefficient.

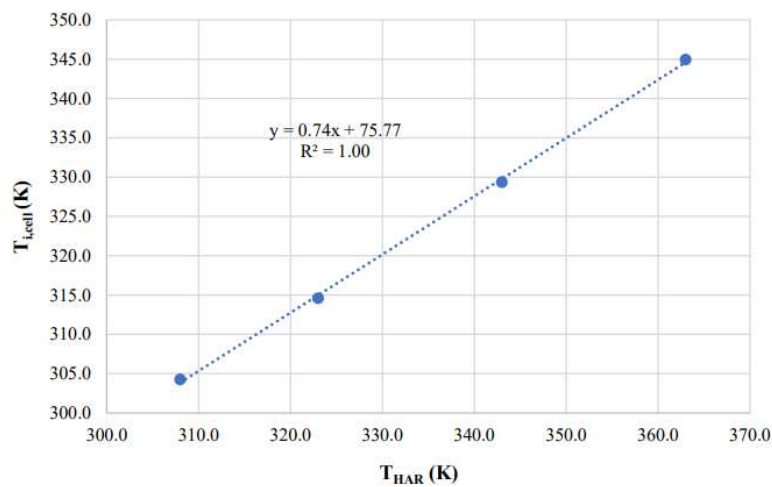


Figure S.2 – Correlation used to calculate $T_{i,cell}$ based on data presented in table S.1

SCHEMATIC REPRESENTING EXCEL SOLUTION TOOL

The model can be run using an excel solution tool which has a user-friendly interface so that even those without the required technical expertise can operate the model. Figure S.3 presents a screenshot of the excel solution tool interface

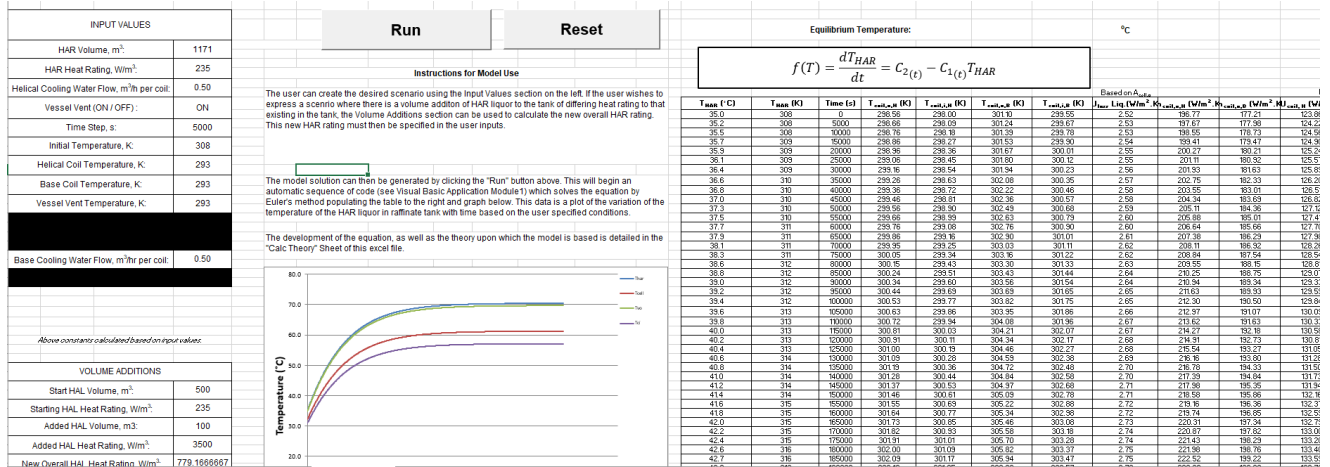


Figure S.3. Schematic that highlights the excel solution tool interface used to solve the non-linear ODE, Eq. (1) to generate a temperate profile for the contents of the BST. The interface is suer friendly so that even those which lack the required technical expertise can operate the model.